# Giant electron-phonon interaction for a prototypical semiconductor interface: Sn / Ge ( 111 ) – ( 3 x 3 )

M. Nair, I. Palacio, A. Mascaraque, E. Michel, A. Taleb-Ibrahimi, Antonio Tejeda, C. González, A. Martín-Rodero, J. Ortega, F. Flores

# A Giant Electron-Phonon Interaction for a Prototypical Semiconductor Interface: Sn/Ge(111)-$(3 \times 3)$

M.N. Nair *,[1,2] I. Palacio *,[2] A. Mascaraque,[3,4] E.G. Michel,[5,6] A. Taleb-Ibrahimi,[2] A. Tejeda,[1,2] C. González,[3,4] A. Martín-Rodero,[7,6] J. Ortega,[7,6] and F. Flores[7,6]

[1]*CNRS, Université Paris-Saclay, Laboratoire de Physique des Solides, 91405 Orsay, France*

[2]*Synchrotron SOLEIL, L'Orme des Merisiers, Saint-Aubin, 91192 Gif sur Yvette, France*

[3]*Departamento de Física de Materiales, Universidad Complutense de Madrid, E-28040 Madrid, Spain*

[4]*Instituto de Magnetismo Aplicado UCM-ADIF, E-28230 Madrid, Spain*

[5]*Departamento de Física de la Materia Condensada, Facultad de Ciencias, Universidad Autónoma de Madrid, E-28049 Madrid, Spain*

[6]*Condensed Matter Physics Center (IFIMAC), Universidad Autónoma de Madrid, E-28049 Madrid, Spain*

[7]*Departamento de Física Teórica de la Materia Condensada, Facultad de Ciencias, Universidad Autónoma de Madrid, E-28049 Madrid, Spain*

(Dated: November 30, 2022)

## Abstract

We report an experimental and theoretical study of the electron-phonon coupling for $\alpha$-Sn/Ge(111), a prototypical triangular lattice surface, closely related to Sn/Si(111)-$\sqrt{3}\times\sqrt{3}$, where recent experimental evidence has found superconductivity [1]. We concentrate our study on the $(3\times3)$-phase of $\alpha$-Sn/Ge(111) that appears between 150 K and 120 K and has a well-known geometry with a half-filled electronic band around the Fermi energy. We show that this surface presents a giant electron-phonon interaction that can be considered at least as partially responsible of the different phases that this system shows at very low temperature. Our theoretical results indicate that indeed the electron-phonon interaction in $\alpha$-Sn/Ge(111)-$(3\times3)$ is unusually large, since we find that $\lambda$, the electron mass enhancement for the half-filled band, is $\lambda = 1.3$. This result is in good agreement with the experimental value obtained from high-resolution angle resolved photoemission spectroscopy measurements, which yield $\lambda = 1.45 \pm 0.1$.


## I. INTRODUCTION

Low dimensional solids have been widely studied during the last years due to their exotic properties [2]. Surfaces are a prominent example, since the reduction of dimensionality from 3D to 2D enhances the importance of fluctuations and entropic effects as well as the role played by electronic correlations in surface states in competition with the degree of coupling between those surface states and the lattice phonons. The variety of surface phenomena encompasses Mott phases, Charge Density Waves, Thouless-Kosterlitz phases, magnetism and superconductivity [1–13].

The $\alpha$-Sn/Si(111) and $\alpha$-Sn/Ge(111) surfaces, obtained by covering a Si or Ge substrate with 0.33 monolayers of Sn, have been widely studied due to their interesting and complex physical behavior. Recently, Weitering *et al.* [1] have observed superconductivity associated with the Sn/Si(111)-$(\sqrt{3}\times\sqrt{3})R30^\circ$ surface states. On the other hand, calculations made for K/Si(111):B-$(\sqrt{3}\times\sqrt{3})R30^\circ$ [14] suggest that for Si-dangling bonds the strength of the electron-phonon (*e-ph*) interaction is very similar to the electron-electron (*e-e*) repulsion, indicating that also in $\alpha$-Sn/Si(111) there might be a close competition between the repulsive *e-e* and attractive *e-ph* interactions [1, 15]. An important *e-ph* interaction associated with partially occupied surface bands has also been observed in Si(111)-$(7\times7)$ ($\lambda = 1.06$ [16]) and in Ge/Si-$(5\times5)$ ($\lambda \simeq 0.53$ [17]). Electron-phonon coupling is thus an important element

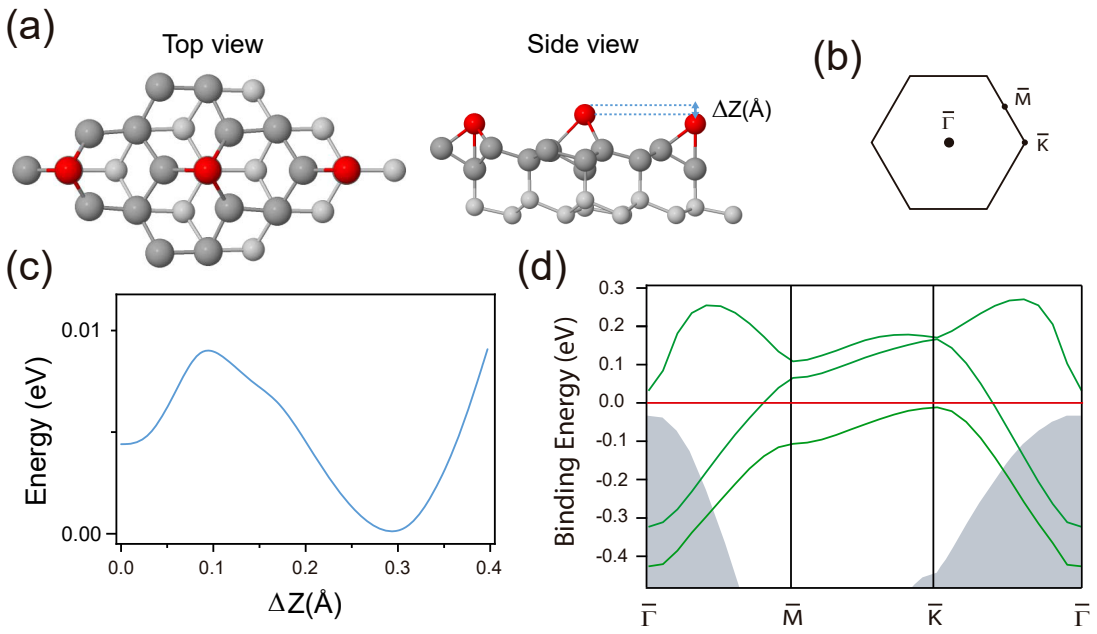


FIG. 1. (a) Top and side views of the Sn/Ge(111)-(3 × 3) surface. (b) Surface Brillouin zone. (c) Energy per (3 × 3)-unit cell associated with the (3×3)-distortion; $\Delta Z = (\Delta z_{up} - \Delta z_{down})$, where $\Delta z_{up}$, $\Delta z_{down}$ are the vertical displacements of the up and down Sn atoms. (d) DFT surface bands; the shaded areas represent the projection of the bulk bands and the red line at 0 eV indicates the Fermi energy $E_F$.

to accurately describe semiconducting surfaces with metallic two-dimensional surface states, and to understand a possible superconductor state and other phase transitions [1, 15, 18, 19].

In this paper we analyze the (3 × 3)-phase appearing between 150 K and 120 K [4, 6] at the $\alpha$-Sn/Ge(111) paradigmatic surface with a combined experimental and theoretical approach to elucidate the importance of the *e-ph* coupling, poorly studied in the past. The (3 × 3) phase has a well-known structure that allows us to perform an accurate analysis of its *e-ph* properties. Our theoretical results indicate that in this surface the *e-ph* interaction is unusually large, $\lambda = 1.3$, in good agreement with the value of $\lambda = 1.45$ found by ARPES experiments. We conclude that the strengths of the *e-ph* and *e-e* interactions are comparable, indicating that the *e-ph* interaction should play an important role in the stabilization of the low temperature phases of $\alpha$-Sn/Ge(111) [4].

## II. ELECTRONIC SURFACE BANDS AND PHONONS

Sn atoms occupy T4 sites of the Ge(111) substrate in the Sn/Ge(111)-(3×3) reconstruction, which is characterized by a vertical distortion, so that one of the three Sn atoms in the unit cell is at a higher position than the other two, see Figure 1a. The interface presents three surface bands. One of them is completely filled and is related to the dangling bond state of the Sn atom moving up. The dangling bond states of the two Sn down atoms create the two other surface states; a bonding combination of those dangling bonds is associated with the metallic band crossing the Fermi energy [7, 20]. Figure 1d shows the three surface bands as calculated with DFT (see Supplemental Material, SM) while the bands below the Fermi energy measured with ARPES are shown in Figure 2a. Notice that the theoretical bandwidth of the metallic band below $E_F$ is around 0.3 eV, while the experimental width of this band is around 0.2 eV. This is probably due to the *e-e* interaction which, as discussed in the SM, yields a band narrowing effect of around 1/1.6, close to the experimental value.

We are interested in calculating the *e-ph* coupling associated with the "active" half-occupied band and the surface phonons of the Sn/Ge(111)-(3×3) surface, assuming that the active band has the measured photoemission bandwidth. As discussed in reference [21], we find three different phonon surface modes associated with the following displacements of the three Sn-atoms of the (3×3)-unit cell along the direction ($z$) perpendicular to the surface: $\vec{u}_1 = (1,1,1)/\sqrt{3}$ ; $\vec{u}_2 = (1,-1,0)/\sqrt{2}$ and $\vec{u}_3 = (-1,-1,2)/\sqrt{6}$. The first mode, $\vec{u}_1$, only introduces a rigid displacement of the three electron surface bands. The second mode, $\vec{u}_2$, interacts weakly with the bonding state of the half-occupied band due to its symmetry. The crucial mode interacting with the "active" band is $\vec{u}_3$, which introduces the same distortion appearing at the $(3 \times 3)$ phase, see below.

Figure 1c shows the energy per $(3 \times 3)$ unit cell along the distortion path defined by the trajectory $(\sqrt{3} \times \sqrt{3})R30^\circ \rightarrow (3 \times 3)$, where the $(\sqrt{3} \times \sqrt{3})R30^\circ$ corresponds to a flat structure with equivalent Sn atoms, as calculated using DFT-techniques (see SM). The down-atoms move to a very good approximation 1/2 of the displacement associated with the up-atom, $\Delta z_{down} \simeq -0.5\Delta z_{up}$ [22]. As expected, the energy minimum appears for the (3×3)-structure with $\sim 5$ meV lower energy [4, 20, 22, 23] than the $(\sqrt{3} \times \sqrt{3})R30^\circ$ structure, and for a relative displacement, $\Delta Z_0 = \Delta z_{up} - \Delta z_{down}$, of 0.29 Å [7, 20]. The $\vec{u}_3$-phonon mode is associated with the potential around that minimum. Calculations and

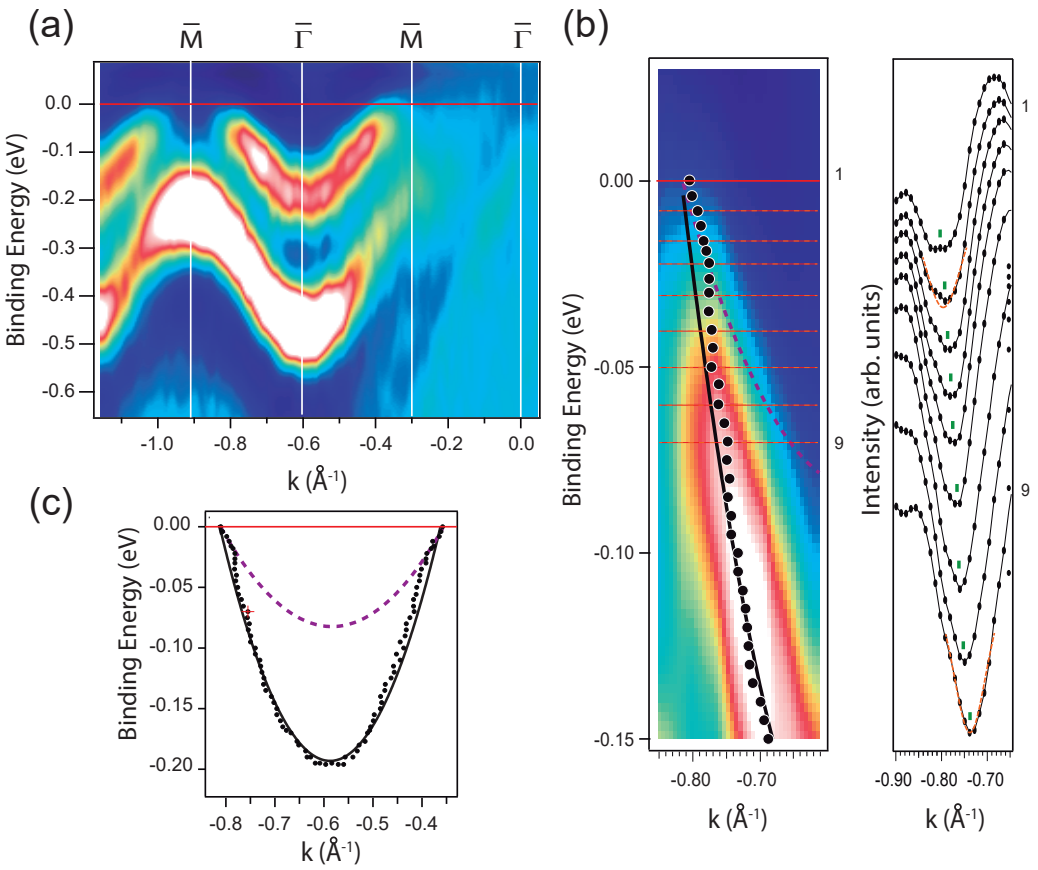


FIG. 2. (a) Second derivative of the ARPES data along the $\overline{\Gamma M}_{3\times3}$ direction in the second BZ (see text). (b) Left panel: Fermi level region from (a). Right panel: Momentum Distribution Curves corresponding to the red lines shown in the left panel. Note that the Momentum Distribution Curves exhibit minima at the location of the band because the figure shows the second derivative of the data. The minima (green tic marks) are fit to Lorenzians (red lines, two fits are shown). The corresponding points appear in the left panel. (c) Experimental points and fit to the bare (black line) and the renormalized (dashed purple line) bands, also shown in panel (b) (left).

He-scattering experiments [21] indicate that the corresponding phonon energy, $\omega_0$, is around 4.3 meV. From our DFT-calculations (Figure 1c), we obtain the potential $V \approx 1/2K\eta^2$ around $\eta = 0$ ($K$ =0.70 eV/Å$^2$), where $\vec{\eta} = \eta(-1,-1,2)/\sqrt{6}$ defines the normal mode along the $\vec{u}_3$ direction. As $\omega_0 = \sqrt{K/M}$, we can also calculate $M = 172\ m_p$ ($m_p$ is the proton mass), in good agreement with [22].

## III. PHOTOEMISSION EXPERIMENTS AND SURFACE BANDS

The fluctuating $(\sqrt{3}\times\sqrt{3})$R30$^0$ reconstruction observed at room temperature freezes into the (3×3)-metallic phase shown in Figure 1 below 150 K. A sharp (3×3) LEED pattern is observed in the 150-120 K range. Below this temperature, however, the intensity of the (3×3) spots weakens [4]. The *e-ph* interaction can be analyzed experimentally by looking at the mass enhancement effect that this interaction introduces in a metallic band around the Fermi energy. This can be accurately determined by means of angle-resolved photoemission spectroscopy (ARPES) measurements [24–27].

We have explored with ARPES the electron mass enhancement associated with the *e-ph* interaction in the 120-150 K temperature range. Figure 2a shows the second derivative of the ARPES data along the $\overline{\Gamma M}_{3\times3}$ direction, where $\overline{\Gamma}$ belongs to the second Brillouin zone. The surface presents two bands, one completely filled band associated with the up atoms and a metallic band related to the down atoms. The detail of the region of the metallic band closer to the Fermi level (Figure 2b) shows that the electronic band does not follow the parabolic dispersion of the band at higher binding energies characterized by the bare effective mass $m_0$. The spectral weight in the two branches of the parabola centered around -0.6 Å$^{-1}$ is not equivalent as often happens in photoemission, due to matrix element effects [28]. Close to the Fermi level, a kink develops in the metallic band, the slope of the band decreases and the effective mass is affected by the *e-ph* coupling in such a way that $m^* = (1+\lambda)m_0$. $\lambda$ can be obtained from the experimental values of $m_0$ and $m^*$ with no further assumption. We have therefore determined the band dispersion (dots in Figures 2b,c) from a fit of the Momentum Distribution Curves to Lorentzian peaks. Once the experimental dispersion was accurately determined, the data were fitted to two parabolas in order to extract $m_0$ and $m^*$. Figure 2c shows that the renormalized parabola fits both branches of experimental data, thus providing a great confidence in the determination. A perfect agreement is however not expected since the state does not follow an ideal parabolic dispersion in the considered energy range, as evident from the theoretical bands (Figure 1d). From these fittings, the *e-ph* mass enhancement parameter is determined to be $\lambda = 1.45 \pm 0.1$, a very large value when compared to the usual values of $\lambda$ in other surfaces [29].

## IV. ELECTRON-PHONON INTERACTION. CALCULATION OF $g$ AND $\lambda$

We analyze theoretically the *e-ph* interaction by means of the following Holstein Hamiltonian [30]:

$$\hat{H} = \sum_{i\sigma} \epsilon_0 \hat{n}_{i\sigma} + \sum_{ij\sigma} T_{ij} \hat{c}^+_{j\sigma} \hat{c}_{i\sigma} + \sum_i \omega_0 \hat{b}^+_i \hat{b}_i + \sum_i g(\hat{b}^+_i + \hat{b}_i)(\hat{n}_{i\uparrow} + \hat{n}_{i\downarrow} - 1) \ , \tag{1}$$

where a local $i$-phonon, the $\vec{u}_3$ mode, with $\omega_0 = 4.3$ meV [21] is coupled to the "active" orbital associated with the half-filled band. In this equation, the creation, $\hat{c}^+_{i\sigma}$, and the anihilation, $\hat{c}_{i\sigma}$, operators, as well as $\hat{n}_{i\sigma} = \hat{c}^+_{i\sigma}\hat{c}_{i\sigma}$, are fermion operators associated with the $i$-bonding orbital of the half-filled band, characterized by the hopping interactions $T_{ij}$; while $\hat{b}^+_i$ and $\hat{b}_i$ are the boson operators associated with the $\vec{u}_3$-phonon.

In this second quantization formalism, the normal mode displacement $\eta_i$ is given by

$$\sqrt{\frac{1}{(2M\omega_0)}}(\hat{b}^+_i + \hat{b}_i) \ ,$$

(with $\hbar = 1$), $M = 172\ m_p$ being the effective mass of the $\vec{u}_3$-phonon mode [31, 32]; on the other hand, the electronic level associated with the $i$-bonding orbital is shifted by the phonon mode, $\eta_i$, as follows:

$$\delta E_i = \frac{\partial E_i}{\partial \eta_i}\eta_i = \frac{\partial E}{\partial \eta}\sqrt{\frac{1}{(2M\omega_0)}}(\hat{b}^+_i + \hat{b}_i) \ ,$$

assuming $\partial E_i/\partial \eta_i$ site independent. This equation shows that

$$g = \frac{\partial E}{\partial \eta}\sqrt{\frac{1}{(2M\omega_0)}} \ ; \tag{2}$$

we calculate $\partial E/\partial \eta$ and $g$, starting from the $(3 \times 3)$-ground state of the system, and introducing a small displacement, $\delta\eta$, for all the Sn atoms (in the $3 \times 3$ unit cell), following the $\vec{u}_3$-phonon mode. Using DFT techniques, we calculate $\partial E_0/\partial(\Delta Z)$, $E_0$ being the energy shift between the up and down surface bands, and $\Delta Z$ the vertical distance between up and down Sn atoms. Since the down atoms associated with the metallic band move 1/3 of the total displacement between up and down Sn atoms, we take $\delta E = \frac{1}{3}\delta E_0$; moreover, the shift in the vertical distance, $\delta(\Delta Z)$, between up and down Sn atoms is given by $\delta(\Delta Z) = \sqrt{\frac{3}{2}}\delta\eta$;

these equations show that $\frac{\partial E}{\partial \eta} = \frac{1}{\sqrt{6}} \frac{\partial E_0}{\partial(\Delta Z)}$. Our calculations yield: $\frac{\delta E_0}{\delta(\Delta Z)} = 0.85$ eV/Å and $g$ = 16.8 meV.

It is interesting to realize that this value of $\frac{\partial E_0}{\partial Z}$ is close to, but a little larger than, the one calculated taking $\Delta E_0$ and $\Delta Z$ from the difference between the $\sqrt{3} \times \sqrt{3}$ and $3 \times 3$ structures: in our calculations (see Figs. 1d and S1 in SM) $\Delta E_0 = 0.20$ eV and $\Delta Z_0 = 0.29$ Å, so that $\frac{\Delta E_0}{\Delta Z_0} = 0.69$ eV/Å; in the calculations of [20] $\frac{\Delta E_0}{\Delta Z_0} = 0.73$ eV/Å.

The *e-ph* interaction can be described by means of an *e-ph* self-energy, $\Sigma(\omega)$ [32], in such a way that $m^*/m_0 = 1 - d\Sigma(\omega = 0)/d\omega$, with $d\Sigma(\omega = 0)/d\omega = -\lambda$. We first obtain $\Sigma_{ii}(\omega) \approx \Sigma(\omega)$ for small $\omega$ using second-order perturbation theory in the *e-ph* interaction $g$, and neglecting the off-diagonal self-energies contributions: $\Sigma_{ij}(\omega) \approx 0$ for $i \neq j$. This approach yields (see SM):

$$\Sigma^{(2)}(\omega) = -2g^2\rho_0\omega/\omega_0 \qquad (\omega \ll \omega_0) \tag{3}$$

where $\rho_0$ is the spin local density of states associated with the half-filled electron band. Then, the *e-ph* mass enhancement parameter $\lambda = -d\Sigma(\omega \to 0)/d\omega$, in second order perturbation theory, is given by $\lambda^{(2)} = 2g^2\rho_0/\omega_0$.

The spin local density of states $\rho_0$ is obtained using the experimental evidence of Figure 2c, where the bare two-dimensional surface band shows a parabolic behaviour below $E_F$; this two-dimensional band yields a constant density of states, so that $\rho_0 \approx 2.5$ eV$^{-1}$ because there are 0.5 electrons per spin in a bandwidth of 0.2 eV. Then, with $g = 16.8$ meV and $\omega_0 = 4.3$ meV, $\lambda^{(2)} \approx 0.32$; this value is quite small as compared to the experimental evidence shown above, $\lambda = 1.45 \pm 0.1$, suggesting that contributions beyond the second order perturbation theory are very important.

In order to go beyond second order perturbation theory in the electron-phonon interaction, $g$, we follow references [30, 33, 34] where the half-filled Holstein Hamiltonian of equation (1) has been analyzed as a function of $g$ for some particular values of $\omega_0$ and $\rho_0$. In these works the lattice model of equation (1) is mapped into an associated impurity level that is embedded in a lattice by means of a Dynamical Mean Field Theory Numerical Renormalization Group (DMFT-NRG) calculation. Of particular interest for our case is the calculation in those references, as a function of $g$, of the quasi-particle weight $Z = (1 - d\Sigma(\omega = 0)/d\omega)^{-1}$ associated with the impurity density of states at the Fermi level ($\omega = 0$); this quantity provides $\lambda = -d\Sigma(\omega = 0)/d\omega = (1 - Z)/Z$ which is shown in the Supplemental Material as

a function of $g\,(\rho_0/\omega_0)^{1/2}$. Notice that is this representation we have changed the abscissa from $g$ to $g\,(\rho_0/\omega_0)^{1/2}$ because in the limit of small $g$ it is found that

$$\lambda^{(2)} = -d\Sigma^{(2)}(\omega = 0)/d\omega = 2\left(g\,(\rho_0/\omega_0)^{1/2}\right)^2 \ ;$$

in this way, for small $g$, $\lambda^{(2)}$ shows a universal behaviour as a function of $g\,(\rho_0/\omega_0)^{1/2}$. Moreover, plotting $\lambda$ as a function of $g\,(\rho_0/\omega_0)^{1/2}$ for the particular values of $\rho_0$ and $\omega_0$ discussed in the DMFT-NRG calculations [30, 33, 34] shows a similar behaviour, see Fig. S2 in the SM, suggesting that to a good approximation in the DMFT-NRG solution of the half-filled Holstein Hamiltonian $\lambda$ is a universal function of $g\,(\rho_0/\omega_0)^{1/2}$.

As an independent check to this conjecture, we have analyzed the case of an impurity embedded in a semi-infinite 1-dimensional spinless chain with nearest neighbors hopping elements, $T_0$, and a local *e-ph* interaction in the last site of the chain: in this model we neglect the posible off-diagonal self-energy terms between different sites, $\Sigma_{ij}(\omega) = 0, i \neq j$, appearing in the lattice of our initial system. Solving numerically this semi-infinite 1-dimensional model with the *e-ph* interaction localized in the impurity is, however, a formidable task in the strong coupling regime, so that in our analysis we have calculated $\lambda$ for a cluster of 6 sites (see SM for details).

A general view of our results is presented in Figure 3, where $\lambda$ and $\lambda^{(2)}$ are shown as a function of $g/\sqrt{\omega_0 T_0}$ for $T_0/\omega_0 = 6$, 8, 10 and 12. These results show that $\lambda/\lambda^{(2)} \approx 1$ for $g/\sqrt{\omega_0 T_0} < 0.6$, while $\lambda/\lambda^{(2)}$ increases steeply for $g/\sqrt{\omega_0 T_0} > 1.0$. In particular, taking $g =$ 16.8 meV and $\omega_0 = 4.3$ meV, from our previous calculations, and choosing $T_0/\omega_0 = 9.7$, a value of $g/\sqrt{\omega_0 T_0} = 1.24$ is obtained; this leads to $\lambda^{(2)} = 0.32$, as calculated above in the second order result, and to $\lambda \approx 1.1$ to all orders in $g$. Thus, this simple model shows a very important increase in the value of $\lambda$, much closer to the experimental result, due to the high orders contributions of $g$. This increase in $\lambda$ is also accompanied by an important increase in the average number of phonons in the ground state of our system: $< n_{ph} > \approx 3.5$, this number indicating that there is a large fluctuation of the phonon mode as corresponds to a strong electron-phonon interaction. We should say that this simple model has been used to check the validity of the universal behaviour of $\lambda$ as a function of $g(\rho_0/\omega_0)^{1/2}$; trying to calculate $\Sigma(\omega)$ for $\omega \gtrsim \omega_0$ is beyond the scope of this simple case.

Moreover, Figure 3 also shows that $g/\sqrt{\omega_0 T_0}$ is a convenient parameter for representing $\lambda$ and $\lambda^{(2)}$ as a function of the *e-ph* interaction, $g$, because for the different values of $T_0/\omega_0$,

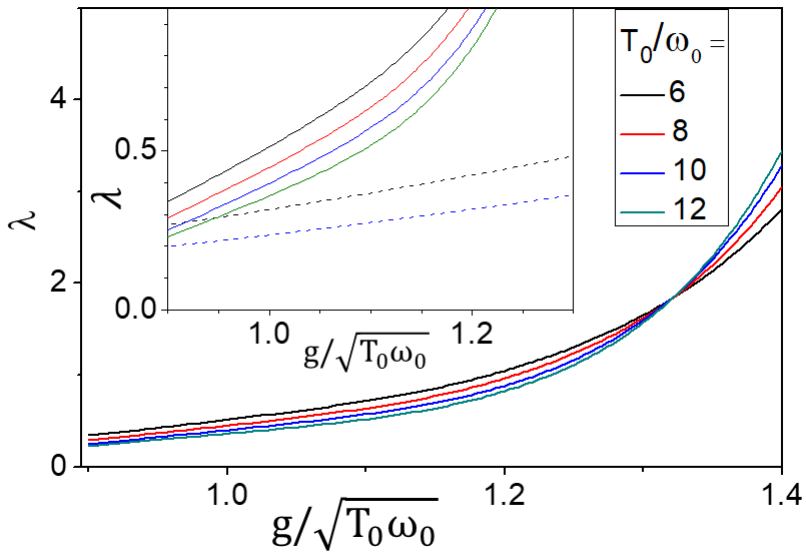


FIG. 3. $\lambda = -d\Sigma_{ii\sigma}(\omega \to 0)/d\omega$ as a function of $g/\sqrt{\omega_0 T_0}$ for the cluster model (see text) for different values of $T_0/\omega_0$. The inset shows $\lambda$ in a different scale; the dotted lines correspond to $\lambda^{(2)}$ for $T_0/\omega_0 = 6$ and 10.

$\lambda$ presents a very similar behavior, indicating that up to a reasonable approximation $\lambda$ is a universal function of $g/\sqrt{\omega_0 T_0}$; notice that in the limit of the semi-infinite chain, the curves shown in Figure 3 should converge, for small $g$, to the function $\lambda = 2\left(g\sqrt{\rho_0/\omega_0}\right)^2$ with $\rho_0$ substituting for $1/T_0$; these arguments indicate that for the semi-infinite chain, with $\rho_0$ proportional to $1/T_0$, $\lambda$ is close to a universal function of $g\sqrt{\rho_0/\omega_0}$, at least for $\lambda < 3.0$, confirming the validity of the conjecture deduced from the DMFT-NRG calculations.

Then, for calculating $\lambda$ for Sn/Ge(111)-3×3, we come back to those DMFT-NRG calculations and take for the Hostein Hamiltonian $\rho_0 = 2.5$ eV$^{-1}$, $\omega_0 = 4.3$ meV and $g = 16.8$ meV. This values yield $g\sqrt{\rho_0/\omega_0} = 0.40$ and $\lambda = 1.30 \pm 0.08$ (see SM), a value in good agreement with the results obtained from the PES experiments. We should mention that the Sn/Ge(111)-surface shows an important high order contribution of the *e-ph* interaction because of the small frequency $\omega_0$ and the high density of states $\rho_0$.

## V. DISCUSSION AND CONCLUSIONS

We have found from the experimental evidence that $\lambda = 1.45 \pm 0.1$, a value much larger than the ones found for Si(111)-7×7 [16], and Ge-Si(111)-5×5 [17]; combining this result

with our theoretical value, $\lambda = 1.30$, yields $\lambda = 1.37 \pm 0.10$ which we consider to be a fair approximation to the value of $\lambda$ for the $\alpha$-Sn/Ge(111)-(3×3) surface.

Regarding our theoretical calculation of the *e-ph* interaction, it is worth stressing that that interaction has been analyzed by going "beyond the second order term" in the $g$-coupling parameter. Notice also that in our calculations for the $\alpha$-Sn/Ge(111) surface, $g\sqrt{\rho_0/\omega_0} = 0.40$, and that the second-order calculation in $g$ is only valid for $g\sqrt{\rho_0/\omega_0} < 0.25$ [30]. This suggests that the $\alpha$-Sn/Ge(111) surface is highly non-linear in the *e-ph* coupling, with $< n_{ph} > \approx 3.5$, and that the usual way of defining the quasi-adiabatic effective phonon-induced attraction, measured by $U_{negative} = 2g^2/\omega_0$ [33], should be reconsidered.

At this point we argue as follows: our calculations from the second order approximation yield that $U_{negative} = 2g^2/\omega_0 = \lambda^{(2)}/\rho_0$. Then, we suggest that, in order to include the higher order contributions, it seems convenient to define a renormalized $U_{negative} = \lambda/\rho_0$ which extrapolates the second order limit to higher values of $g$.

It is worth considering now what is the value of $U_{negative}$, as deduced from the value of $\lambda = 1.37 \pm 0.1$. This yields $U_{negative} = \lambda/\rho_0 = 0.55 \pm 0.06$ eV, this quantity being close to, but slightly larger than, the value calculated for the effective *e-e* interaction for the $\alpha$-Sn/Ge(111)-$(3 \times 3)$ surface, $(U - V) \approx 0.43$ eV [4]. From these figures we conclude that the low temperature phases of $\alpha$-Sn/Ge(111), including a possible superconducting state, should appear as a result of a delicate balance between the *e-ph* and *e-e* interactions.

## VI. METHODS

Photoemission experiments were performed at the high-resolution branch of CASSIOPEE beamline at Soleil synchrotron. The ultrahigh vacuum set up couples a surface preparation chamber equipped with LEED and a high-resolution ARPES chamber equipped with a manipulator operating between 400 and 5 K and with a Scienta R4000 electron analyzer having a $\pm 15^0$ acceptance angle. Incoming radiation and the normal to the detector center subtend a 45° angle. In our experiments, we settled the light polarization in the plane defined by these two directions while the detector slit was perpendicular to them. The valence band measurements were performed at $h\nu = 80$ eV. The sample preparation has been described elsewhere [4]. The 0.33 ML Sn surface coverage was calibrated from the Sn 4d/Ge 3d intensity ratio, surface state intensity, and the evolution of the LEED pattern.

In the DFT calculations we have used the QUANTUM ESPRESSO code [35] with the PBE exchange-correlation functional [36] and the Ultrasoft pseudopotentials provided by the code. The $(3 \times 3)$ surface slab was built with 11 Ge layers and 3 Sn adatoms in T4 positions in the upper layer. The dangling bonds of the lowest Ge layer are saturated by H atoms. The lower two Ge-layers and the H atoms are fixed in the simulations. See Supplemental Material for more details.

## ACKNOWLEDGMENTS

This work was supported by the French Agence Nationale de la Recherche (ANR), project SurMott, ref. NT-09-618999. We acknowledge financial support from the Spanish Ministry of Science and Innovation through projects No. MAT2017-88258-R, PID2021-123295NB-I00, PID2020-117024GB-C43, PID2021-125604NB-I00 and No. CEX2018-000805-M (María de Maeztu Programme for Units of Excellence in R&D). We also acknowledge the technical support provided by the Centro de Computación Científica-UAM (CCC-UAM), Project No. BIOFAST. We thank Prof. D. Farías for many helpful discussions.

* These authors contributed equally.

[1] X. Wu, F. Ming, T.S. Smith, G. Liu, F. Ye, K. Wang, S. Johnston and H.H. Weitering, Phys. Rev. Lett. **125**, 117001 (2020).

[2] P.C. Snijders and H.H. Weitering, Rev. Mod. Phys. **82**, 307 (2010).

[3] N.J. DiNardo, T.M. Wong and E.W. Plummer, Phys. Rev. Lett. **65**, 2177 (1990).

[4] R. Cortés, A. Tejeda, J. Lobo-Checa, C. Didiot, B. Kierren, D. Malterre, J. Merino, F. Flores, E.G. Michel and A. Mascaraque, Phys. Rev. B **88**, 125113 (2013).

[5] R. Cortés, A. Tejeda, J. Lobo, C. Didiot, B. Kierren, D. Malterre, E.G. Michel and A. Mascaraque, Phys. Rev. Lett. **96**, 126103 (2006).

[6] J.M. Carpinelli, H.H. Weitering, M. Bartkowiak, R. Stumpf and E.W. Plummer, Phys. Rev. Lett. **79**, 2859 (1997).

[7] J. Avila, A. Mascaraque, E.G. Michel, M.C. Asensio, G. LeLay, J. Ortega, R. Pérez and F. Flores, Phys. Rev. Lett. **82**, 442 (1999).

[8] B. Guster, R. Robles, M. Pruneda, E. Canadell and P. Ordejón, 2D Mater. **6**, 015027 (2019).

[9] T. Aruga, Surf. Sci. Rep. **61**, 283 (2006).

[10] J.M. Kosterlitz and D.J. Thouless, J. Phys. C **6**, 1181 (1973).

[11] B.I. Halperin and D.R. Nelson, Phys. Rev. Lett. **41**, 519 (1978).

[12] T.S. Smith, F. Ming, D.G. Trabada, C. González, D. Soler-Polo, F. Flores, J. Ortega and H.H. Weitering, Phys. Rev. Lett. **124**, 097602 (2020).

[13] G. Li, P. Höpfner, J. Schäfer, C. Blumenstein, S. Meyer, A. Bostwick, E. Rotenberg, R. Claessen and W. Hanke, Nat. Commun. **4**, 1620 (2013).

[14] D.G. Trabada, J.I. Mendieta-Moreno, D. Soler-Polo, F. Flores and J. Ortega, Appl. Surf. Sci. **479**, 260 (2019).

[15] S. Wolf, D. Di Sante, T. Schwemmer, R. Thomale, and S. Rachel, arXiv:2107.03482v1, 7 July 2021.

[16] I. Barke, F. Zheng, A.R. Konicek, R.C. Hatch and F.J. Himpsel, Phys. Rev. Lett. **96**, 216801 (2006).

[17] M. Stoffel, Y. Fagot-Revurat, A. Tejeda, B. Kierren, A. Nicolaou, P. Le Fèvre, F. Bertran, A. Taleb-Ibrahimi and D. Malterre, Phys. Rev. B **86** 195438 (2012).

[18] G. Anemone *et al*, 2D Mater. **7**, 025007 (2020).

[19] N.F. Hinsche and K.S. Thygesen, 2D Mater. **5**, 015009 (2018).

[20] O. Pulci, M. Marsili, P. Gori, M. Palummo, R. Del Sole, A. Cricenti, F. Bechstedt, Appl. Phys. A **85**, 361 (2006).

[21] D. Farías, W. Kamiński, J. Lobo, J. Ortega, E. Hulpke, R. Pérez, F. Flores and E.G. Michel, Phys. Rev. Lett. **91**, 016103 (2003).

[22] R. Pérez, J. Ortega and F. Flores, Phys. Rev. Lett. **86**, 4891 (2001).

[23] S. de Gironcoli, S. Scandolo, G. Ballabio, G. Santoro, E. Tossati, Surf. Sci. **454-56**, 172 (2000).

[24] J. A. Sobota, Y. He, and Z.X. Shen, Rev. Mod. Phys. **93**, 025006 (2021).

[25] M. Hengsberger, D. Purdie, P. Segovia, M. Garnier, and Y. Baer, Phys. Rev. Lett. **83**, 592 (1999).

[26] A. Lanzara, P. V. Bogdanov, X. J. Zhou, S. A. Kellar, D. L. Feng, E. D. Lu, T. Yoshida, H. Eisaki, A. Fujimori, K. Kishio, J.-I. Shimoyama, T. Nodak, S. Uchidak, Z. Hussain and Z.-X. Shen, Nature **412**, 510 (2001).

[27] E.W. Plummer, J. Shi, S.-J. Tang, Eli Rotenberg, S.D. Kevan, Progress in Surface Science

**74**, 251 (2003).

[28] M. Mulazzi, G. Rossi, J. Braun, J. Minar, H. Ebert, G. Panaccione, I. Vobornik, and J. Fujii, Phys. Rev. B **79**, 165421 (2009).

[29] G. Benedek, J. R. Manson and S. Miret-Artés, Phys. Chem. Chem. Phys. **23**, 7575 (2021).

[30] D. Meyer, A.C. Hewson and R. Bulla, Phys. Rev. Lett. **89**, 196401 (2002).

[31] J.M. Ziman, "Electrons and Phonons". Oxford University Press (1960).

[32] G.D. Mahan, "Many-Particle Physics". Springer (2000).

[33] W. Koller, D. Meyer and A.C. Hewson, Phys. Rev. B **70**, 155103 (2004).

[34] A.C. Hewson and D. Meyer, J. Phys. Condens. Matter **14**, 427 (2002).

[35] A. Dal Corso, Computational Material Science **95**, 337 (2014).

[36] J. P. Perdew, K. Burke, and M. Ernzerhof, Phys. Rev. Lett. **77**, 3865 (1996).